

Low-threshold power and tunable integrated optical limiter based on an ultracompact VO₂/Si waveguide

Cite as: APL Photonics 6, 121301 (2021); <https://doi.org/10.1063/5.0071395>

Submitted: 14 September 2021 • Accepted: 17 November 2021 • Accepted Manuscript Online: 17 November 2021 • Published Online: 03 December 2021

 Jorge Parra,  Juan Navarro-Arenas,  Mariela Menghini, et al.



View Online



Export Citation



CrossMark

ARTICLES YOU MAY BE INTERESTED IN

[Silicon photonic beam steering module with backside coupling elements toward dense heterogeneous integration with drive electronics](#)

APL Photonics 6, 116106 (2021); <https://doi.org/10.1063/5.0065210>

[An ITO-graphene heterojunction integrated absorption modulator on Si-photonics for neuromorphic nonlinear activation](#)

APL Photonics 6, 120801 (2021); <https://doi.org/10.1063/5.0062830>

[Nanophotonics-enabled optical data storage in the age of machine learning](#)

APL Photonics 6, 110902 (2021); <https://doi.org/10.1063/5.0065634>

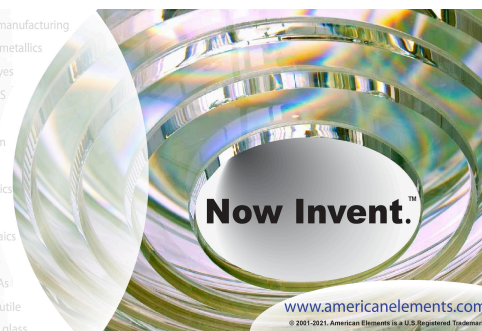


THE ADVANCED MATERIALS MANUFACTURER

yttrium iron garnet glassy carbon beamsplitters fused quartz additive manufacturing
 zeolites III-IV semiconductors gallium lump copper nanoparticles organometallics
 nano ribbons barium fluoride europium phosphors photonics infrared dyes
 epitaxial crystal growth ultra high purity materials transparent ceramics CIGS
 cerium oxide polishing powder surface functionalized nanoparticles MRE grade materials thin film
 sapphire windows Nd:YAG rare earth metals quantum dots osmium scintillation Ce:YAG
 refractory metals laser crystals anode lithium niobate InAs wafers dysprosium pellets MOFs AuNPs
 chalcozenides ZnS CdTe perovskite crystals transparent ceramics

epitaxial crystal growth ultra high purity materials transparent ceramics CIGS
 cerium oxide polishing powder surface functionalized nanoparticles MRE grade materials thin film
 OLED lighting solar energy sputtering targets fiber optics
 h-BN deposition slugs CVD precursors photovoltaics
 metamaterials borosilicate glass YBCO superconductors InGaAs
 indium tin oxide MgF₂ rutile diamond micropowder optical glass

The Next Generation of Material Science Catalogs



Low-threshold power and tunable integrated optical limiter based on an ultracompact VO₂/Si waveguide

Cite as: APL Photon. 6, 121301 (2021); doi: 10.1063/5.0071395
Submitted: 14 September 2021 • Accepted: 17 November 2021 •
Published Online: 3 December 2021



View Online



Export Citation



CrossMark

Jorge Parra,¹ Juan Navarro-Arenas,¹ Mariela Menghini,^{2,3} Maria Recaman,² Jean Pierre-Locquet,²
and Pablo Sanchis^{1,a)}

AFFILIATIONS

¹Nanophotonics Technology Center, Universitat Politècnica de València, Camino de Vera s/n, 46022 Valencia, Spain

²Department of Physics and Astronomy, KU Leuven, Celestijnenlaan 200D, 3001 Leuven, Belgium

³IMDEA Nanociencia, Calle Faraday 9, E28049 Madrid, Spain

^{a)}Author to whom correspondence should be addressed: pabsanki@ntc.upv.es

ABSTRACT

Optical limiters are nonlinear devices that encompass applications from device protection to activation functionalities in neural networks. In this work, we report an optical limiter on silicon photonics based on an ultracompact VO₂/Si waveguide. Our 20- μ m-long experimental device features a thermal tunable threshold power of only \sim 3.5 mW while being spectrally broadband. Our work provides a new pathway to achieve integrated optical limiters for dense and low-power photonic integrated circuits.

© 2021 Author(s). All article content, except where otherwise noted, is licensed under a Creative Commons Attribution (CC BY) license (<http://creativecommons.org/licenses/by/4.0/>). <https://doi.org/10.1063/5.0071395>

I. INTRODUCTION

Silicon photonics has been established as a mature and mainstream photonic integrated platform for developing a wide range of applications in the fields of telecom and datacom,¹ quantum computing,² or LiDAR,³ to name a few. Although such achievement has been accomplished, thanks to the broad variety of passive and active building blocks,⁴ to date, there is not a clear approach on how to implement optical limiting devices.

Optical limiters are devices that exhibit a clipped-like input–output power response. Below a certain threshold, the device has a linear response, while for higher values, it becomes nonlinear and saturates the output.⁵ The most straightforward application of optical limiters in photonic integrated circuits is to protect optical devices against hazardous high-power signals, encompassing from conventional photodetectors to emerging all-optical devices. In the latter, devices such as optical memories,^{6,7} non-volatile switches,⁸ or optical synapses⁹ rely on chalcogenide phase change materials.¹⁰ In such devices, the involved phase change amorphization and crystallization processes require tight control of the optical power to avoid permanent damage.¹¹ On the other hand, optical limiters are useful to provide stability from

fluctuations in high-sensitive optical devices, such as microring resonators or cavities.¹² Moreover, the nonlinear transfer function featured by optical limiters finds direct application in new areas such as artificial intelligence or neuromorphics¹³ to perform activation functions such as the clipped rectified linear unit (ReLU).¹⁴

Optical limiting is readily observable in silicon waveguides owing to silicon nonlinearities, such as two-photon absorption (TPA) or free carrier absorption (FCA).¹⁵ However, in a straight waveguide, there is a severe trade-off between threshold power and length. For instance, optical limiting arises for threshold powers of hundreds of milliwatts when using millimeter-long waveguides.^{16–18} Resonant cavities such as microring resonators have been proposed to enhance nonlinear effects and thus reduce the footprint.¹⁹ However, the threshold power remains in the same magnitude as in previous straight waveguides, while the bandwidth is reduced to values below 0.1 nm.

Such values are not compatible with current trends in photonic integrated circuits that move toward reducing both the footprint and energy consumption of devices,^{20,21} reconfigurability,²² and exploitation of dense wavelength-division multiplexing (DWDM) by taking the advantages of parallelism and capacity.^{23,24}

Therefore, integrated optical limiters featuring low-threshold power and the possibility of tunability with spectral broadband in an ultracompact footprint would be beneficial.

A route to achieve such goals could be the integration of new materials into the silicon photonics platform featuring an optical nonlinearity significantly larger than silicon. In this context, vanadium dioxide (VO₂) is a complementary metal–oxide–semiconductor (CMOS)-compatible phase transition oxide exhibiting a unity order change on both real and imaginary parts of its refractive index stemming from the insulator-metal transition (IMT) at around 65 °C.²⁵ Such appealing properties have been exploited in a large variety of nanophotonic devices.²⁶ In the field of integrated photonics, the high contrast and broadband optical properties of VO₂ have been utilized for all-optical modulation and switching applications.^{27–31} Recently, the optical limiting response has been observed in VO₂ thin films^{32,33} and applied to metasurfaces.^{34–36} Here, we demonstrate that the photoinduced IMT can be also leveraged to achieve high-performance optical limiting for integrated photonic waveguide-based applications.

In this Letter, we experimentally demonstrate an ultra-compact VO₂/Si optical limiter on silicon photonics featuring low-threshold power and tunability over a broad spectral response. The optical limiting response is achieved by harnessing the strong change in the absorption of VO₂ that accompanies the IMT and exploiting the gradual insulator to the metal profile along the propagation direction under in-plane photothermal excitation.

II. WORKING PRINCIPLE

A. In-plane photothermal response

Figure 1(a) illustrates the photothermal behavior of a hybrid VO₂/Si waveguide fed by a high-power optical signal. We consider a standard Si waveguide with a thin VO₂ patch of length *L* atop. The

IMT of VO₂ is triggered by evanescent coupling so that the absorbed optical power (*P_{abs}*) in VO₂ acts as a heat source. Due to the in-plane approach, the value of the heat source is related to the absorption strength of the optical mode,

$$\frac{\partial P_{abs}}{\partial z} = P_{in} \alpha \exp(-\alpha z), \tag{1}$$

where *P_{in}* is the input power and α is the propagation loss, with the latter given by

$$\alpha = \frac{4\pi\kappa_{eff}}{\lambda}, \tag{2}$$

where κ_{eff} is the effective extinction coefficient and λ is the working wavelength. Because the absorption strength is not constant along the propagation direction (*z* axis) and thus the heat source, there is a temperature gradient in that direction. This temperature gradient translates into a phase-change gradient; the portion VO₂ material above the IMT temperature (*T_{IMT}*) will transition to metal, while the remaining portion of the patch will stay insulating.

According to previous experimental works,^{29,30} the relation between the length of the metal fragment (*L_m*) and the optical power can be approximated as

$$L_m \approx \eta \ln\left(\frac{P_{in}}{P_{th}}\right), \tag{3}$$

where η is a term relating to the thermo-optical efficiency of the structure and depends on both optical and thermal properties of the hybrid waveguide.

The different states that the hybrid waveguide can undergo are depicted in Fig. 1(b). For low optical power below the threshold power, VO₂ is insulating as the temperature in the patch is below the *T_{IMT}*. High optical power is required to obtain a full insulator–metal transition since the temperature profile in the whole VO₂ layer

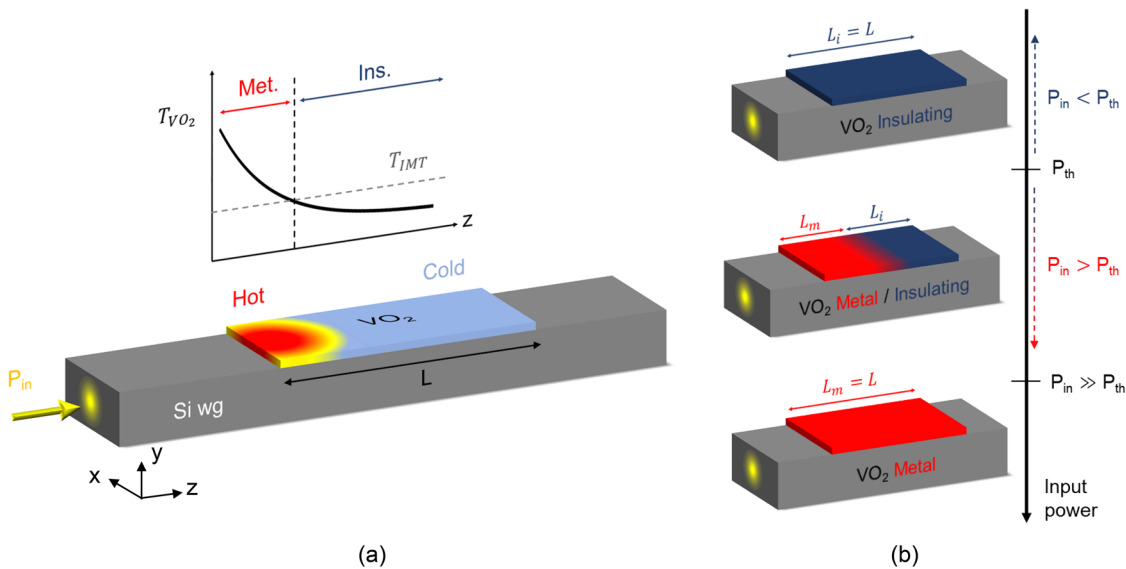


FIG. 1. (a) Illustration of VO₂ heating in a hybrid VO₂/Si waveguide using an in-plane photothermal approach. (b) States of the VO₂ patch as the input power in the waveguide is increased.

needs to be above T_{IMT} . Yet, in both cases, the output–input optical response of the hybrid waveguide is linear and is given by the propagation loss in the insulating (α_i) and metallic (α_m) case, respectively.

On the other hand, for intermediate states comprised of a fraction of metal and insulator VO₂, the optical response can be described as

$$P_{out} = P_{in} \exp[-(\alpha_m - \alpha_i)L_m - \alpha_i L]. \quad (4)$$

Thereby, for such states, the optical response of the hybrid waveguide becomes nonlinear due to L_m and its dependence on the optical power [see Eq. (3)].

B. Optical limiting condition

Optical limiting is achieved when the induced optical losses match the increase in the optical power when this exceeds the threshold power. In this case, the output is constant regardless of the input value. This can be achieved by leveraging the nonlinear response of VO₂/Si found in the intermediate optical states [see Eq. (4)]. To this end, the following condition needs to be met:

$$P_{th} \exp(-\alpha_i L) = P_{in} \exp[-(\alpha_m - \alpha_i)L_m - \alpha_i L]. \quad (5)$$

As a result, we obtain that the value of L_m fulfilling the optical limiting condition for a specific optical power is

$$L_{m,OL} = \frac{\ln(P_{in}/P_{th})}{\alpha_m - \alpha_i}. \quad (6)$$

Finally, by comparing Eqs. (3) and (6), we obtain that the photothermal efficiency term should be

$$\eta_{OL} = \frac{1}{\alpha_m - \alpha_i}. \quad (7)$$

In Fig. 2(a), the value of η with respect to $\alpha_m - \alpha_i$ in the different regimes is shown. The optical limiting condition is comprised of overlimiting (red region) and underlimiting (blue region) regimes. Such regimes arise when η does not match the value given by Eq. (7). The optical responses for the three regimes are plotted in Fig. 2(b). When the VO₂ layer is mix of metal and insulator ($I \rightarrow M$), the output increases (underlimiting) or decreases (overlimiting) depending

on whether the induced optical losses are lower [$\eta(\alpha_m - \alpha_i) < 1$] or higher [$\eta(\alpha_m - \alpha_i) > 1$], respectively, than the increase in the input power.

On the other hand, the photothermal efficiency is related to the light–matter interaction between the optical mode and the VO₂. Hence, different strategies can be followed to control the value of η in VO₂/Si waveguides to fulfill Eq. (7), such as changing the distance between the silicon waveguide and the VO₂ patch or varying the thickness of the VO₂. The photothermal efficiency will also depend on the polarization of the propagating mode.

III. RESULTS

Our hybrid waveguide is based on a standard $480 \times 220 \text{ nm}^2$ Si waveguide with a 40-nm-thick VO₂ layer on top separated by a 60 nm spacer formed by a 10-nm-thick silicon oxide layer plus a 50-nm-thick SiN hardmask. The SiN layer is required for the planarization of the surface. To obtain a patterned polycrystalline VO₂ layer, a 40-nm-thick amorphous VO₂ layer was grown by molecular beam epitaxy (MBE) with a subsequent lift-off process to remove the undesired regions. Finally, an *ex situ* annealing process was carried out at 400 °C in forming gas. The refractive index of the deposited VO₂ at telecom wavelengths and for different temperatures is reported in Fig. 3. Film characterization was carried out by spectroscopy ellipsometry and following the same deposition process. The chip was covered with 700 nm of SiO₂ by plasma-enhanced chemical vapor deposition (PECVD). The length of the device is only 20 μm . Figure 4(a) shows an optical microscope image of the fabricated VO₂/Si waveguide.

The optical and photothermal parameters for that type of waveguide are $\alpha_i \approx 0.91 \text{ dB}/\mu\text{m}$, $\alpha_m \approx 1.61 \text{ dB}/\mu\text{m}$, and $\eta \approx 1.06 \mu\text{m}/\text{dB}$ at $\lambda = 1550 \text{ nm}$ and for transverse-electric (TE) polarization.³⁰ Therefore, our device was expected to be close to the optical limiting condition according to Eq. (7) with a small underlimiting response.

The experimental setup used for characterizing the optical limiter is shown in Fig. 4(b). A tunable continuous-wave (CW) laser together with an erbium-doped fiber amplifier (EDFA) working in the telecom C-band was used as the light source. Fiber-to-chip coupling was achieved using standard TE grating couplers. The temperature of the chip during measurements was controlled using

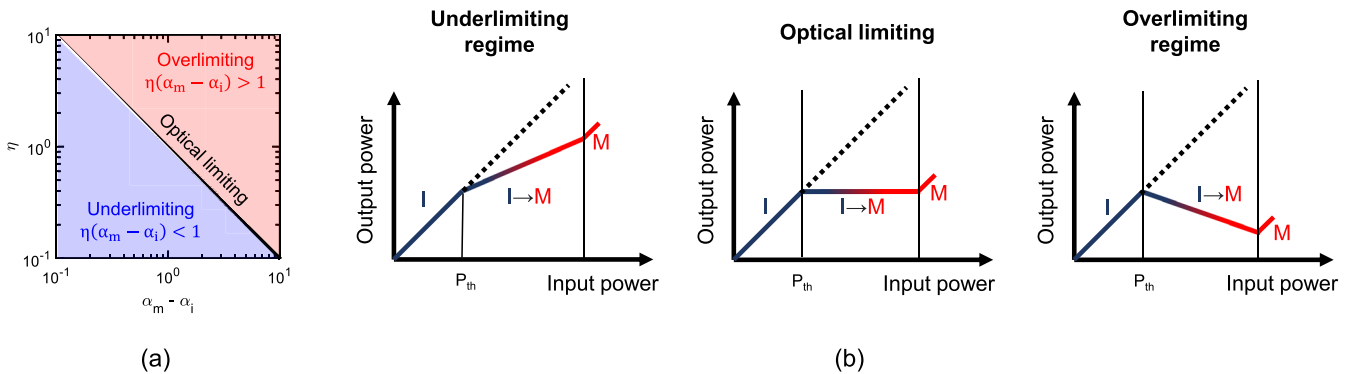


FIG. 2. (a) Optical limiting condition in a VO₂/Si waveguide using an in-plane photothermal approach. (b) Optical response of the hybrid waveguide for the different regimes.

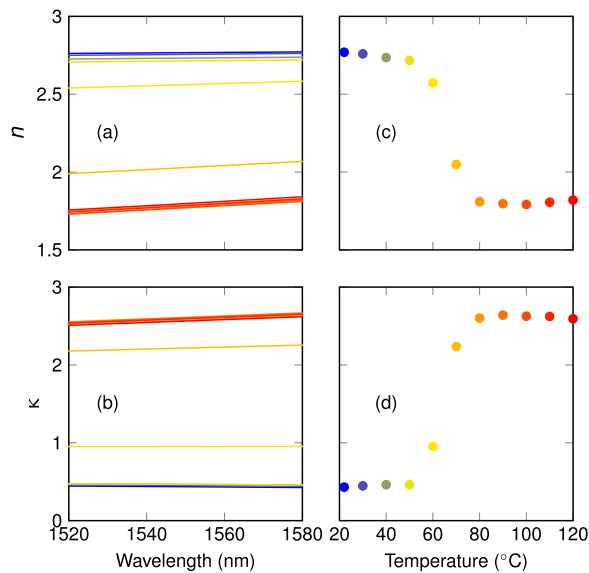


FIG. 3. Refractive index ($n + j\kappa$) of VO_2 thin film as a function of the wavelength and for different temperatures during a heating cycle. (a) Real and (b) imaginary parts of the refractive index spectrum. (c) Real and (d) imaginary parts of the refractive index at 1565 nm as a function of the temperature.

a Peltier device. Finally, the output power was measured using a high-sensitivity photodetector.

The power limiting response was characterized by setting the wavelength of the laser and increasing the optical power. Figure 5 shows the power response of a reference silicon waveguide without VO_2 and the hybrid waveguide acting as an optical limiter at different temperatures. Input and output optical power values are given on-chip. The reference waveguide was characterized to discard a loss contribution from silicon nonlinear effects. In such a way, a linear response was obtained [see Fig. 5(a)]. Therefore, considering the values of optical power, the nonlinear and limiting response of the hybrid waveguide owns to the photothermal induced IMT of VO_2 [Figs. 5(b) and 5(c)].

To fit the experimental values, we model the optical response by using Eqs. (3) and (4). A fair agreement is found between the experiment (dots) and the proposed model (solid lines). Therefore, optical saturation occurs due to the discussed relationship between the gradual metallic change of the VO_2 layer along the propagation direction and the optical power [see Eq. (6)]. Our device features a low-threshold power of ~ 3.5 mW near room temperature [see Fig. 5(b)] alongside a plateau in the response, which is indicative of being near the optical limiting condition [see Fig. 2(b)], for a range of input powers of around 7 dB.

Since the IMT is photothermally triggered, our optical limiter provides also the possibility of tuning its response. Biasing the temperature of the VO_2 near (far) the IMT reduces (increases) its threshold power. To prove this point, the temperature of the chip was increased to 50°C [Fig. 5(c)], near the IMT ($\sim 65^\circ\text{C}$), with the Peltier device. In this manner, the threshold power was reduced down to ~ 2 mW since a smaller increase in temperature was required to trigger the IMT. Consequently, the input range, i.e., the input power values comprised between the threshold power and the maximum measured power [see Fig. 2(b)], increased up to ~ 10 dB. On the other hand, the photothermal efficiency was slightly improved ($\eta \approx 1.2 \mu\text{m}/\text{dB}$) because the difference between T_{IMT} and the background temperature was decreased.

The spectral response of the proposed optical limiter is mainly limited by the wavelength dependence of the propagation losses [see Eqs. (2) and (7)]. In this regard, a remarkable advantage of the proposed optical limiter device is that it benefits from the low dispersion of VO_2 at telecom wavelengths [see Figs. 3(a) and 3(b)], thus providing a broadband response in VO_2/Si waveguides. To showcase this feature, we characterized the spectral response of our hybrid waveguide under low- and high-power signals as shown in Fig. 6, i.e., $P_{\text{in}} < P_{\text{th}}$ and $P_{\text{in}} \geq P_{\text{th}}$, respectively. The wavelength dependence of the input power is due to the EDFA. We measured an optical limiting bandwidth of around 15 nm. It should be highlighted that the measured spectral range was limited by our EDFA and not by the bandwidth of the device, which should be larger due to the non-resonant operation. When the low-power signal at the input of the hybrid waveguide remains far below the threshold, the device works

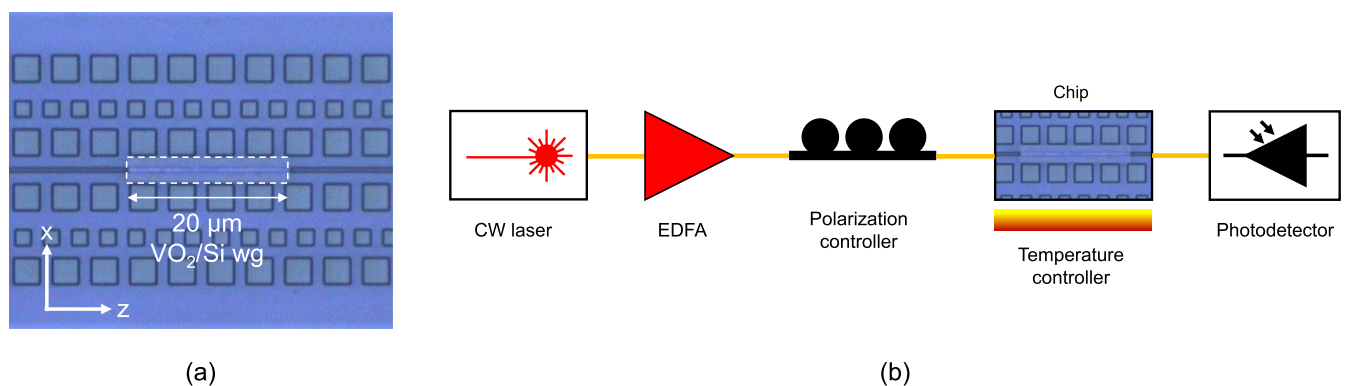


FIG. 4. (a) Optical microscope image of the optical limiter. The squares are made of silicon. (b) Experimental setup.

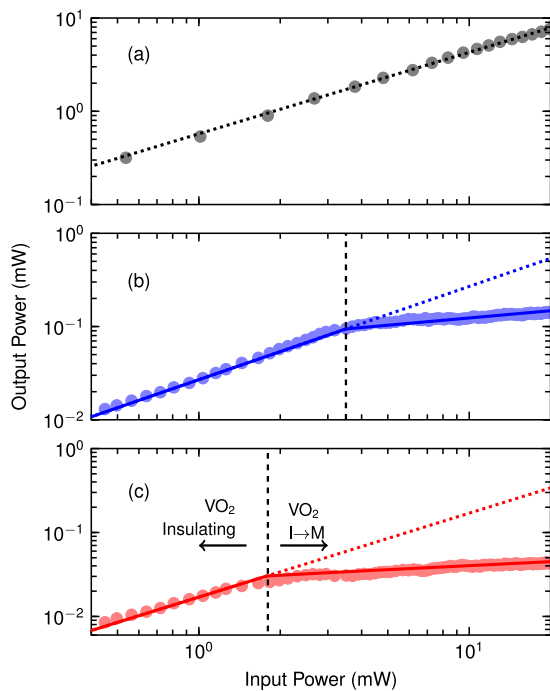


FIG. 5. Optical response of the (a) reference Si waveguide and (b) and (c) hybrid VO₂/Si waveguide setting the temperature of the chip at (b) 30 °C and (c) 50 °C. Experimental values (dots) are given on-chip at 1565 nm. Solid lines stand for fitted data. Dotted lines show the extrapolated behavior of the optical limiter if it would have remained in the linear regime (full insulating VO₂).

on the linear regime (full insulating VO₂), and therefore, the output is proportional to the input and both responses have a similar shape. On the other hand, for the high-power signal, the hybrid waveguide is driven to the optical limiting condition (metal/insulator VO₂)

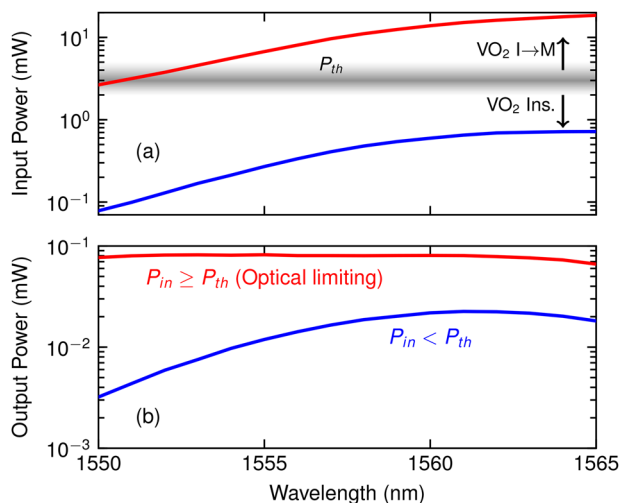


FIG. 6. Spectral response of the device under below-threshold (blue) and above-threshold (red) signals. (a) Input and (b) output power as a function of the wavelength. The shaded region in (a) stands for the threshold power. For larger values, the device limits the power at the output and flattens the spectrum. Values are given on-chip and at 30 °C.

because the input power exceeds the limiter threshold. Hence, the output is saturated resulting in a flattening of the spectral response (Fig. 6).

IV. CONCLUSION

In summary, we have demonstrated that the strong optical nonlinear response of VO₂ can be leveraged for achieving ultra-compact and broadband optical limiters on silicon photonics with tunable performance. On-chip efficient thermal biasing could be easily achieved using low-loss microheaters,^{37,38} while the threshold power of the device could be engineered by doping the VO₂ in order to modify the transition temperature.^{39–41} On the other hand, the turn-on time of such a device under photothermal excitation is expected to be around a few microseconds.^{29,30} Since VO₂ is a CMOS-compatible material, our study opens up opportunities to include such a building block onto dense, low power consumption, and DWDM photonic integrated applications.

ACKNOWLEDGMENTS

This study was supported by Grant Nos. PID2019-111460GB-I00 and FPU17/04224 funded by MCIN/AEI/10.13039/501100011033 and, by “ESF Investing in your future”; Grant funded by FEDER/Ministerio de Ciencia e Innovación-Agencia Estatal de Investigación/Ref.ICTS-2017-28-UPV-9; PROMETEO Program (Ref.2019/123)-Generalitat Valenciana; and Action co-financed by the European Union through the European Regional Development Fund (ERDF) operational program for the Valencian Community 2014-2020. The authors also thank David Zurita for his help with the experimental setup and Pía Homm for the sample preparation.

AUTHOR DECLARATIONS

Conflict of Interest

The authors have no conflicts to declare.

DATA AVAILABILITY

The data that support the findings of this study are available from the corresponding author upon reasonable request.

REFERENCES

- G. T. Reed, G. Mashanovich, F. Y. Gardes, and D. J. Thomson, “Silicon optical modulators,” *Nat. Photonics* **4**, 518–526 (2010).
- J. Wang, F. Sciarrino, A. Laing, and M. G. Thompson, “Integrated photonic quantum technologies,” *Nat. Photonics* **14**, 273–284 (2020).
- M. J. R. Heck, “Highly integrated optical phased arrays: Photonic integrated circuits for optical beam shaping and beam steering,” *Nanophotonics* **6**, 93–107 (2017).
- S. Y. Siew, B. Li, F. Gao, H. Y. Zheng, W. Zhang, P. Guo, S. W. Xie, A. Song, B. Dong, L. W. Luo, C. Li, X. Luo, and G.-Q. Lo, “Review of silicon photonics technology and platform development,” *J. Lightwave Technol.* **39**, 4374–4389 (2021).
- L. W. Tutt and T. F. Boggess, “A review of optical limiting mechanisms and devices using organics, fullerenes, semiconductors and other materials,” *Prog. Quantum Electron.* **17**, 299–338 (1993).

- ⁶C. Ríos, M. Stegmaier, P. Hosseini, D. Wang, T. Scherer, C. D. Wright, H. Bhaskaran, and W. H. P. Pernice, "Integrated all-photonic non-volatile multi-level memory," *Nat. Photonics* **9**, 725–732 (2015).
- ⁷X. Li, N. Youngblood, C. Ríos, Z. Cheng, C. D. Wright, W. H. Pernice, and H. Bhaskaran, "Fast and reliable storage using a 5 bit, nonvolatile photonic memory cell," *Optica* **6**, 1 (2019).
- ⁸P. Xu, J. Zheng, J. K. Doylend, and A. Majumdar, "Low-loss and broadband non-volatile phase-change directional coupler switches," *ACS Photonics* **6**, 553–557 (2019).
- ⁹Z. Cheng, C. Ríos, W. H. P. Pernice, C. D. Wright, and H. Bhaskaran, "On-chip photonic synapse," *Sci. Adv.* **3**, e1700160 (2017).
- ¹⁰M. Wuttig, H. Bhaskaran, and T. Taubner, "Phase-change materials for non-volatile photonic applications," *Nat. Photonics* **11**, 465–476 (2017).
- ¹¹E. Gemo, S. G.-C. Carrillo, C. R. De Galarreta, A. Baldycheva, H. Hayat, N. Youngblood, H. Bhaskaran, W. H. P. Pernice, and C. D. Wright, "Plasmonically-enhanced all-optical integrated phase-change memory," *Opt. Express* **27**, 24724 (2019).
- ¹²W. Bogaerts, P. De Heyn, T. Van Vaerenbergh, K. De Vos, S. Kumar Selvaraja, T. Claes, P. Dumon, P. Bienstman, D. Van Thourhout, and R. Baets, "Silicon microring resonators," *Laser Photonics Rev.* **6**, 47–73 (2012).
- ¹³B. J. Shastri, A. N. Tait, T. Ferreira de Lima, W. H. P. Pernice, H. Bhaskaran, C. D. Wright, and P. R. Prucnal, "Photonics for artificial intelligence and neuromorphic computing," *Nat. Photonics* **15**, 102–114 (2021).
- ¹⁴C. Nwankpa, W. Ijomah, A. Gachagan, and S. Marshall, "Activation functions: Comparison of trends in practice and research for deep learning," [arXiv:1811.03378](https://arxiv.org/abs/1811.03378) [cs.LG] (2018).
- ¹⁵R. M. Osgood, Jr., N. C. Panoiu, J. I. Dadap, X. Liu, X. Chen, I.-W. Hsieh, E. Dulkeith, W. M. Green, and Y. A. Vlasov, "Engineering nonlinearities in nanoscale optical systems: Physics and applications in dispersion-engineered silicon nanophotonic wires," *Adv. Opt. Photonics* **1**, 162 (2009).
- ¹⁶E. Dulkeith, Y. A. Vlasov, X. Chen, N. C. Panoiu, and R. M. Osgood, Jr., "Self-phase-modulation in submicron silicon-on-insulator photonic wires," *Opt. Express* **14**, 5524 (2006).
- ¹⁷I.-W. Hsieh, X. Chen, J. I. Dadap, N. C. Panoiu, R. M. Osgood, S. J. McNab, and Y. A. Vlasov, "Ultrafast-pulse self-phase modulation and third-order dispersion in Si photonic wire-waveguides," *Opt. Express* **14**, 12380 (2006).
- ¹⁸A. Gil-Molina, I. Aldaya, J. L. Pita, L. H. Gabrielli, H. L. Fragnito, and P. Dainese, "Optical free-carrier generation in silicon nano-waveguides at 1550 nm," *Appl. Phys. Lett.* **112**, 251104 (2018).
- ¹⁹S. Yan, J. Dong, A. Zheng, and X. Zhang, "Chip-integrated optical power limiter based on an all-passive micro-ring resonator," *Sci. Rep.* **4**, 6676 (2015).
- ²⁰R. Amin, R. Maiti, Y. Gui, C. Suer, M. Miscuglio, E. Heidari, R. T. Chen, H. Dalir, and V. J. Sorger, "Sub-wavelength GHz-fast broadband ITO Mach-Zehnder modulator on silicon photonics," *Optica* **7**, 333 (2020).
- ²¹M. Ono, M. Hata, M. Tsunekawa, K. Nozaki, H. Sumikura, H. Chiba, and M. Notomi, "Ultrafast and energy-efficient all-optical switching with graphene-loaded deep-subwavelength plasmonic waveguides," *Nat. Photonics* **14**, 37–43 (2020).
- ²²W. Bogaerts, D. Pérez, J. Capmany, D. A. B. Miller, J. Poon, D. Englund, F. Morichetti, and A. Melloni, "Programmable photonic circuits," *Nature* **586**, 207–216 (2020).
- ²³P. Dong, "Silicon photonic integrated circuits for wavelength-division multiplexing applications," *IEEE J. Sel. Top. Quantum Electron.* **22**, 370–378 (2016).
- ²⁴D. Kong, H. Xin, K. Kim, Y. Liu, L. K. Oxenlowe, P. Dong, and H. Hu, "Intra-datacenter interconnects with a serialized silicon optical frequency comb modulator," *J. Lightwave Technol.* **38**, 4677–4682 (2020).
- ²⁵M. Currie, M. A. Mastro, and V. D. Wheeler, "Characterizing the tunable refractive index of vanadium dioxide," *Opt. Mater. Express* **7**, 1697 (2017).
- ²⁶S. Cuffey, J. John, Z. Zhang, J. Parra, J. Sun, R. Orobtcouk, S. Ramanathan, and P. Sanchis, "VO₂ nanophotonics," *APL Photonics* **5**, 110901 (2020).
- ²⁷K. J. Miller, R. F. Haglund, and S. M. Weiss, "Optical phase change materials in integrated silicon photonic devices: Review," *Opt. Mater. Express* **8**, 2415 (2018).
- ²⁸H. M. K. Wong, Z. Yan, K. A. Hallman, R. E. Marvel, R. P. Prasankumar, R. F. Haglund, and A. S. Helmy, "Broadband, integrated, micron-scale, all-optical Si₃N₄/VO₂ modulators with pJ switching energy," *ACS Photonics* **6**, 2734–2740 (2019).
- ²⁹K. Shibuya, K. Ishii, Y. Atsumi, T. Yoshida, Y. Sakakibara, M. Mori, and A. Sawa, "Switching dynamics of silicon waveguide optical modulator driven by photothermally induced metal-insulator transition of vanadium dioxide cladding layer," *Opt. Express* **28**, 37188 (2020).
- ³⁰J. Parra, T. Ivanova, M. Menghini, P. Homm, J.-P. Locquet, and P. Sanchis, "All-optical hybrid VO/Si waveguide absorption switch at telecommunication wavelengths," *J. Lightwave Technol.* **39**, 2888–2894 (2021).
- ³¹K. A. Hallman, K. J. Miller, A. Baydin, S. M. Weiss, and R. F. Haglund, "Sub-picosecond response time of a hybrid VO₂:silicon waveguide at 1550 nm," *Adv. Opt. Mater.* **9**, 2001721 (2021).
- ³²M. Maaza, D. Hamidi, A. Simo, T. Kerdja, A. K. Chaudhary, and J. B. Kana Kana, "Optical limiting in pulsed laser deposited VO₂ nanostructures," *Opt. Commun.* **285**, 1190–1193 (2012).
- ³³M. Maaza, B. D. Ngom, M. Achouri, and K. Manikandan, "Functional nanostructured oxides," *Vacuum* **114**, 172–187 (2015).
- ³⁴A. Howes, Z. Zhu, D. Curie, J. R. Avila, V. D. Wheeler, R. F. Haglund, and J. G. Valentine, "Optical limiting based on Huygens' metasurfaces," *Nano Lett.* **20**, 4638–4644 (2020).
- ³⁵L. Hsu and A. Ndao, "Diffraction-limited broadband optical meta-power-limiter," *Opt. Lett.* **46**, 1293 (2021).
- ³⁶C. Wan, Z. Zhang, J. Salman, J. King, Y. Xiao, Z. Yu, A. Shahsafi, R. Wambold, S. Ramanathan, and M. A. Kats, "Ultrathin broadband reflective optical limiter," *Laser Photonics Rev.* **15**, 2100001 (2021).
- ³⁷L. Yu, Y. Yin, Y. Shi, D. Dai, and S. He, "Thermally tunable silicon photonic microdisk resonator with transparent graphene nanoheaters," *Optica* **3**, 159 (2016).
- ³⁸J. Parra, J. Hurtado, A. Griol, and P. Sanchis, "Ultra-low loss hybrid ITO/Si thermo-optic phase shifter with optimized power consumption," *Opt. Express* **28**, 9393 (2020).
- ³⁹K. Shibuya, M. Kawasaki, and Y. Tokura, "Metal-insulator transition in epitaxial V_{1-x}W_xO₂ (0 ≤ x ≤ 0.33) thin films," *Appl. Phys. Lett.* **96**, 022102 (2010).
- ⁴⁰J. G. Ramirez, T. Saerbeck, S. Wang, J. Trastoy, M. Malnou, J. Lesueur, J.-P. Crocombette, J. E. Villegas, and I. K. Schuller, "Effect of disorder on the metal-insulator transition of vanadium oxides: Local versus global effects," *Phys. Rev. B* **91**, 205123 (2015).
- ⁴¹K. Miyazaki, K. Shibuya, M. Suzuki, H. Wado, and A. Sawa, "Correlation between thermal hysteresis width and broadening of metal-insulator transition in Cr- and Nb-doped VO₂ films," *Jpn. J. Appl. Phys., Part 1* **53**, 071102 (2014).